RSC Advances

PAPER

View Article Online
View Journal | View Issue

Cite this: *RSC Adv.*, 2021, **11**, 13130

Nanostructure and thermoresponsiveness of poly(*N*-isopropyl methacrylamide)-based hydrogel microspheres prepared *via* aqueous free radical precipitation polymerization†

Yuichiro Nishizawa, [a] Haruka Minato, [a] Takumi Inui,[a] Ikuma Saito,[a] Takuma Kureha, [c] Mitsuhiro Shibayama, [d] Takayuki Uchihashi *[ef] and Daisuke Suzuki *[ab]

Thermoresponsive hydrogel microspheres (microgels) are smart materials that quickly respond to external stimuli, and their thermoresponsiveness can be tuned by varying the constituent chemical species. Although uniformly sized microgels can be prepared *via* aqueous free radical precipitation polymerization, the nanostructure of the obtained microgels is complex and remains unclear so far. In the present study, the nanostructure and thermoresponsiveness of poly(*N*-isopropyl methacrylamide) (pNIPMAm)-based microgels, which have a volume-transition temperature of ~43 °C, were evaluated mainly using temperature-controllable high-speed atomic force microscopy. These observations, which are characterized by high spatio-temporal resolution, revealed that the pNIPMAm microgels have a peculiar heterogeneous structure, for example a core–shell and non-thermoresponsive nanostructure in the core region, that originates from the precipitation polymerization process. Furthermore, it was found that the adsorption concentration of the microgels on the substrate is one of the keys for controlling their thermoresponsiveness. These findings can be expected to advance the design of new materials such as thermoresponsive nanosheets and stimuli-responsive coatings.

Received 2nd March 2021
Accepted 28th March 2021

DOI: 10.1039/d1ra01650d

rsc.li/rsc-advances

Introduction

Hydrogel microspheres (microgels) are water-swollen, soft polymeric microspheres that consist of cross-linked hydrophilic (amphiphilic) polymer chains.[1–4] Owing to the hydrated nature of their polymer chains, microgels have high biocompatibility and colloidal stability when compared to rigid particles like polystyrene or silica nanoparticles. The size of a typical microgel is in the range of several tens of nanometers to several micrometers, and thus, microgels can respond instantly to external stimuli such as changes in temperature, pH, and solvent. Due to their desirable properties, microgels have found applications, not only in a dispersed state, for example as carriers for drug-delivery systems,[5–7] in molecular separations,[8–11] and in functional catalysts,[12–14] but also in assembled states, for example as cell scaffolds,[15,16] sensors,[17,18] emulsifiers,[19,20] and actuators.[21–23]

The first reported microgels were thermoresponsive poly(*N*-isopropyl acrylamide) (pNIPAm)-based microgels cross-linked with *N*,*N*′-methylenebis(acrylamide) (BIS).[24] These microgels have a volume-phase-transition temperature (VPTT) of ~32 °C and their physicochemical properties change quickly when the temperature increases beyond this point.[1] The VPTT of microgels can be controlled by varying the constituent chemical species, such as (meth)acrylamide analogues,[1,25,26] *N*-vinylcaprolactam (VCL),[27,28] and oligo(ethylene glycol) methylester (meth)acrylates.[9,10,29] This is especially notable in the case of *N*-isopropyl methacrylamide (NIPMAm), which differs from NIPAm only by a single methyl group at the α-position, where the obtained pNIPMAm microgels have a VPTT of ~43 °C.[30–38] The VPTT of microgels can also be tuned *via* the copolymerization of NIPMAm with other chemical species, such as NIPAm or VCL.[39–42]

Thermoresponsive microgels are mainly synthesized *via* aqueous free radical precipitation polymerization in water. In

[a]*Graduate School of Textile Science & Technology, Shinshu University, 3-15-1 Tokida, Ueda, Nagano 386-8567, Japan*
[b]*Research Initiative for Supra-Materials, Interdisciplinary Cluster for Cutting Edge Research, Shinshu University, 3-15-1 Tokida, Ueda, Nagano 386-8567, Japan*
[c]*Graduate School of Science & Technology, Hirosaki University, 3, Bunkyo-cho, Hirosaki, Aomori 036-8561, Japan*
[d]*Neutron Science and Technology Center, Comprehensive Research Organization for Science and Society, 162-1 Shirakata Tokai, Ibaraki 319-1106, Japan*
[e]*Department of Physics, Structural Biology Research Center, Graduate School of Science, Nagoya University, Furo-cho, Chiksusa-ku, Nagoya, Aichi 464-8602, Japan*
[f]*Exploratory Research Center on Life and Living Systems, National Institutes of Natural Science, 5-1 Higashiyama, Myodaiji, Okazaki, Aichi 444-8787, Japan*

† Electronic supplementary information (ESI) available: Height movies of pNIPMAm microgels with different adsorption concentrations. See DOI: 10.1039/d1ra01650d

this system, microgels are formed *via* the self-assembly of phase-separated polymer chains.[1,43,44] In order to control the structure of the microgels, it is therefore important to understand the reactivity ratio between the main monomer and the cross-linker. To date, the structural elucidation of p(NIPAm-*co*-BIS) microgels has mainly been attempted using scattering techniques[45–47] and microscopy,[48,49] and it has been concluded that these microgels show heterogeneous core–shell structures as the BIS cross-linker is consumed faster than the NIPAm.[50] Recently, using temperature-controllable high-speed atomic force microscopy (TC-HS-AFM), we have revealed that cross-linked pNIPAm microgels exhibit a non-thermoresponsive nano-structure in the core region.[44,51–55]

In general, the chemical structure of the monomer determines the reactivity ratio and thus, different reactivity ratios (*i.e.*, monomers) might cause structural changes in the microgels. For instance, the calculated reactivity ratio in the presence of BIS is lower for acrylamide than for methacrylamide (*e.g.*, acrylamide: $r_1 = 0.48$; BIS: $r_2 = 2.0$; methacrylamide: $r_1 = 0.85$; BIS: $r_2 = 0.84$),[56,57] suggesting that the structure of the microgels composed of acrylamide or methacrylamide derivatives is different.

To clarify the internal structure of microgels composed of pNIPMAm, methacrylamide derivatives, we investigated the detailed nanostructure and thermoresponsiveness of pNIPMAm-based microgels, prepared by precipitation polymerization, using a combination of electron microscopy, static/dynamic light scattering techniques, and TC-HS-AFM.

Results and discussion

Microgel preparation and characterization in the dispersed state

Initially, the pNIPMAm microgels were prepared by aqueous free radical precipitation polymerization using BIS as the cross-linker. A field emission scanning electron microscopy (FE-SEM) analysis showed that uniformly sized pNIPMAm-based microgels with a size of 224 nm in the dried state were obtained (Fig. 1(a)). Subsequently, the thermoresponsive behavior of the microgels was evaluated by dynamic light scattering (DLS). As the temperature was increased above 31 °C, the hydrodynamic diameter (D_h) of the microgels (322 nm) gradually decreased to an almost equilibrium size (209 nm) at 50 °C (Fig. 1(b)). The volume transition temperature, defined as the temperature where the rate of change in volume reaches its maximum, was determined to be 45.5 °C. To examine the structure of the microgels in their swollen and deswollen states in aqueous solution, static light scattering (SLS) measurements were conducted (Fig. 1(c)). The scattering profiles at 25 °C and 50 °C are described well by a fuzzy-sphere form factor (eqn (1)).[45] The thickness of the fuzzy layer(σ_{surf}) and the radius of the particle where the scattering-length-density profile decreased to half the core density (R) of the swollen microgels was 18 nm and 115 nm, whereas those of the deswollen microgels were 4.4 nm and 90 nm, respectively. This result suggests that the pNIPMAm microgels have, as previously reported,[26,58] a heterogeneous core–shell type structure in the swollen state. The electrophoretic mobility (EPM), which reflects the surface properties of a microgel, was -1.65×10^{-8} m^2 V^{-1} s^{-1} at 25 °C and -3.12×10^{-8} m^2 V^{-1} s^{-1} at 50 °C. In the case of pNIPAm microgels with the same BIS composition (D_h: 296 nm), σ_{surf}, R, and the EPM were 13 nm, 107 nm, and -2.02×10^{-8} m^2 V^{-1} s^{-1} (swollen state) meanwhile 8.1 nm, 83 nm, and -2.65×10^{-8} m^2 V^{-1} s^{-1} (deswollen state).[53] Wedel *et al.* have reported similar results and concluded that pNIPMAm microgels possess more homogeneous network structures than pNIPAm microgels.[25] The larger EPM of the pNIPMAm microgels in the swollen state at 25 °C suggests that the cross-linking density of the surface of pNIPMAm microgels is lower than that of pNIPAm microgels, which is probably due to self-crosslinking in the latter.[33]

TC-HS-AFM observations of a single microgel

Next, the thermoresponsive behavior and nanostructure of a single pNIPMAm microgel were directly visualized using TC-HS-AFM, which allows low-invasiveness, real-time observation of the nanodynamics with controlling the solution temperature over a range from ~25 °C to 50 °C.[53,59] Here, the temperature was increased by 2 °C min^{-1}, while height and phase images, which show differences in the physical properties, and 3D images constructed from the height images were obtained at a rate of 1 s per frame (Fig. 2 and Movie S1†). Due to the evaporation of the sample solution, the thermoresponsive behavior of the microgels was observed separately over a temperature range of ~25 °C to ~40 °C (Fig. 2(a)) and ~40 °C to ~50 °C (Fig. 2(b)). The phase images show a low-density shell layer with a width of 20 nm, which could not be observed in the

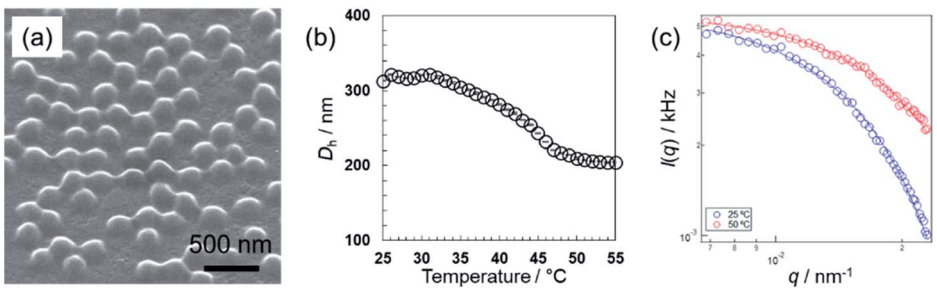

Fig. 1 (a) FE-SEM images of pNIPMAm-based microgels. (b) Temperature dependence of the hydrodynamic diameter. (c) Scattering curves at 25 °C and 50 °C obtained from SLS measurements. The solid line shows the calculated value derived from eqn (1).

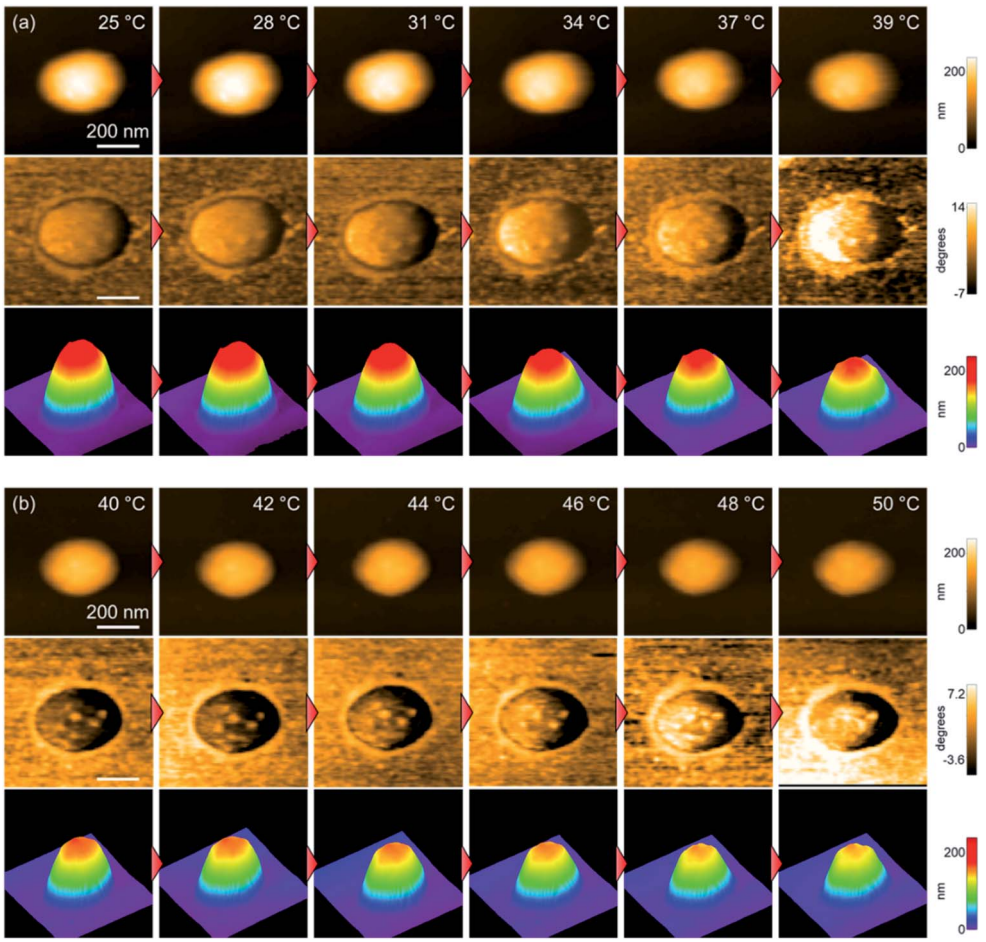

Fig. 2 TC-HS-AFM images showing how the height (top), phase (middle), and constructed 3D images (bottom) of the pNIPMAm microgels vary with temperature. (a) 25–40 °C, (b) 40–50 °C.

height images. The height (D_{height}) and width of the microgel were obtained from the height images (Fig. 3(a)). In agreement with the results of the DLS measurements, the microgel height decreased above 31 °C, but in contrast to D_h, the magnitude of change in the height is lower (Fig. 3(b)). Thus, the microgel height did not match D_h at each temperature (*e.g.*, the height, width, and D_h at 25 °C were 233 nm, 347 nm, and 313 nm, respectively). The differences between the DLS and TC-HS-AFM measurements can be attributed to the effect of adsorption and deformation: the amphiphilic microgels were adsorbed on a hydrophobized mica substrate with deformation to minimize the contact area between water and the substrate.[60] The width of the microgels, including the low-density shell layer, measured from the phase images (D_{phase}) remained almost constant with increasing temperature although the width of the core region in the phase images (D_{core}), along with D_{height}, also decreased (Fig. 3(c) and (d)). This result indicates that the shell layer was strongly adsorbed onto the substrate. Thus, the changes in height of the core regions were not matched by the changes in D_h, which reflects the whole spherical microgel dispersed in aqueous solution. The ratio of the highly cross-linked core region of the pNIPMAm microgels (D_{core}/D_{phase}) was 0.78 ($N = 3$), whereas that of the pNIPAm microgels was 0.69 ($N = 3$).[53] This result indicates that the cross-linking distribution of the pNIPMAm microgels is more homogeneous as well as the result of SLS measurement and previous study.[25] The more homogeneous network structure may be caused by the comparable reactivity ratios of methacrylamide derivatives and BIS.[56,57] Moreover, non-thermoresponsive spherical domains with a width of 50–70 nm, similar to those of pNIPAm microgels,[53] were observed in the phase images (Fig. 3(e) and (f)). This nanoarchitecture indicates that BIS-rich polymer chains, formed in the early stages of the precipitation polymerization process, aggregated in multiple steps during the nucleation process and formed highly cross-linked spherical domains.[44,53] Therefore, we concluded that the heterogeneous core–shell and non-thermoresponsive domains are formed in the microgels *via* precipitation polymerization even when the reactivity of the chemical species is different.

Thermoresponsiveness of microgels with different adsorption concentrations

To clarify the effect that the adsorption density has on the thermoresponsive behavior of the pNIPMAm microgels, TC-HS-AFM observations of samples with different concentrations of

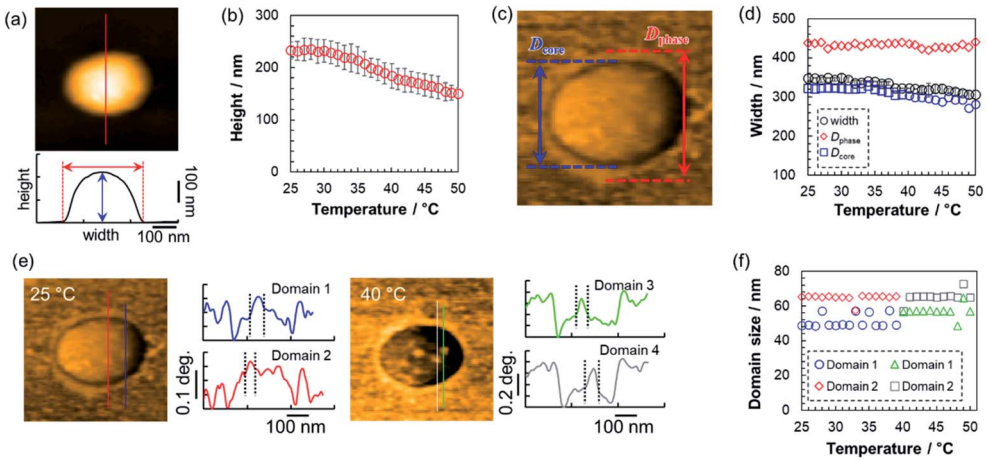

Fig. 3 (a) Method to evaluate the height and width of the pNIPMAm-based microgels and (b) the change in microgel height with increasing temperature. (c) Definition of D_{phase} and D_{core} in the phase images. (d) Temperature dependence of the width, D_{phase}, and D_{core}. (e) Method to calculate the size of the domains that exist in the core region of the microgels and (f) temperature dependence of each domain size.

adsorbed microgels were performed; for that purpose, a loosely arranged state with a concentration of 5.3 particles per μm^2 (Fig. 4(a) and Movie S2†) and a densely packed state (18.8 particles per μm^2) were examined (Fig. 4(b) and Movie S3†). In the case of the loosely arranged state, where the sample was prepared on the substrate by adsorption of a 1.0 wt% microgel dispersion (isolated state: 0.05 wt%, Fig. 2), the thermoresponsive behavior in relation to the height of each microgel was similar to that of the isolated state (Fig. 4(c)). The decrease in width (347 nm in the isolated state; 271 nm in the loosely

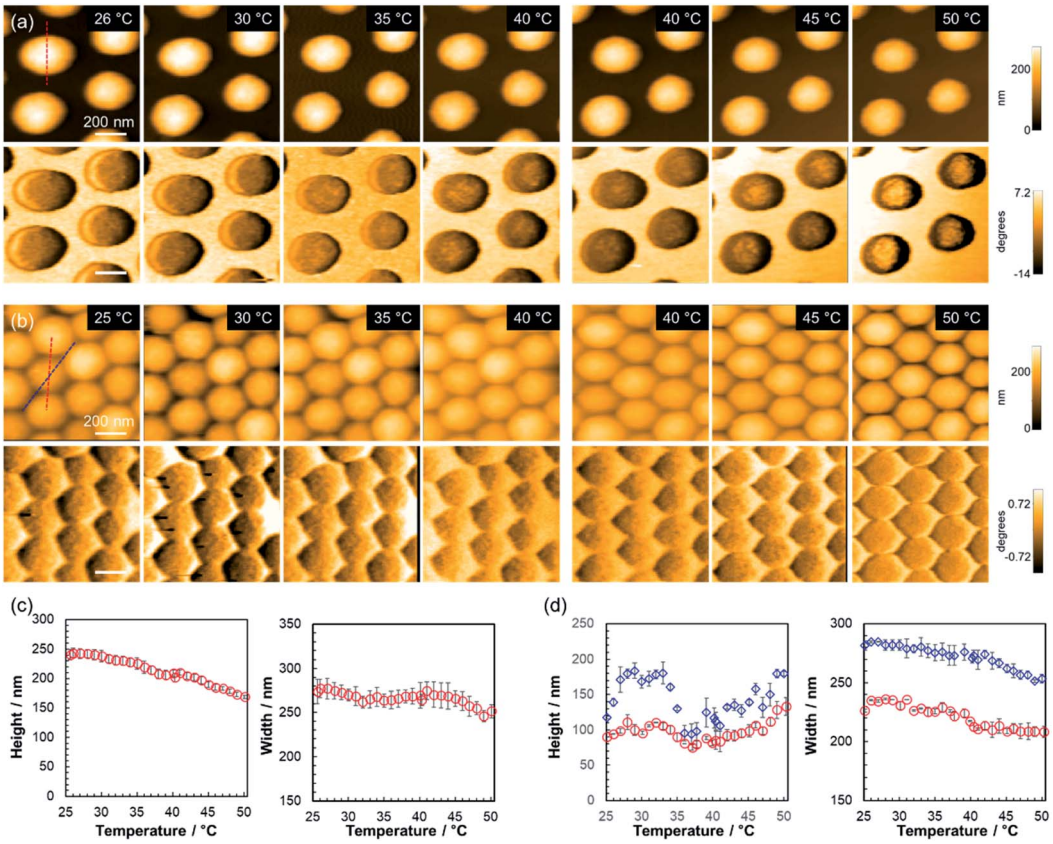

Fig. 4 Temperature dependence of the microgels at different adsorption concentrations. Height images (top) and phase images (bottom) of (a) the loosely arranged state (5.3 particles per μm^2) and (b) the densely packed state (18.8 particles per μm^2). (c) Temperature dependence of the height and width of the microgels corresponding to the red dotted line in (a). (d) Temperature dependence of the height and width between the edge-to-edge (red circles) and vertex-to-vertex (blue diamonds) of a single microgel. The red and blue plots correspond to the red and blue dotted lines in (b), respectively.

arranged state at 25 °C) suggests that the deformation of the microgels on the substrate is suppressed by neighboring microgels.

The densely packed microgels were generated by coating the substrate with a microgel paste prepared by ultracentrifugation of microgel dispersions. In contrast to the loosely arranged sample, the hexagonal shape of the microgels was deformed: the edge-to-edge and vertex-to-vertex distances of a single microgel were 226 nm and 281 nm, respectively at 25 °C (corresponding to the red and blue dotted lines in Fig. 4(b)). The heights were 89 nm and 119 nm at 25 °C between the edges and the vertices of a single microgel, respectively. When the temperature was increased, the height between the sides increased from 89 nm at 25 °C to 110 nm at 32 °C, decreased to 75 nm at 37 °C, and finally increased again to 133 nm at 50 °C. Conversely, the height at the vertices finally reached 180 nm (Fig. 4(d)). Notably, the microgels always maintain a hexagonal structure with increasing temperature. These results suggest that the neighboring microgels are almost in contact at their sides during heating and that the probe could not image the substrate. However, the probe was able to approach the substrate closer near the vertices where the microgels had little contact with each other. Previously the structures of three-dimensional densely packed microgels have been investigated using super-resolution microscopy.[61,62] Conley *et al.* have reported on the structural changes of microgels when the volume fraction of the microgels is increased. Initially, the particle radius decreases while maintaining its shape, indicating that the low-density fuzzy layer of the microgels, which could not be observed by super-resolution microscopy, is compressed and interpenetrated.[62] With increasing volume fraction of the microgels, a deformation of the microgels to a hexagonal-like structure was observed, and finally further reduction of particle radius occurs.[62] Thus, the hexagonally deformed pNIPMAm microgels prepared here by precipitation polymerization should be compressed and interpenetrated when the microgels are packed at high density. In addition, our results revealed that their hexagonal shape was maintained during heating, suggesting that compression and interpenetration of the neighboring microgels suppress the thermoresponsiveness in the x, y direction. The thermoresponsive behavior of isolated and densely packed microgels is illustrated in Scheme 1. These results show that the thermoresponsiveness of microgels can be controlled by varying not only the constituent chemical species, but also by controlling the adsorption state. These findings can be expected to be of use in the design of temperature-responsive 2D assemblies such as cell scaffolds.

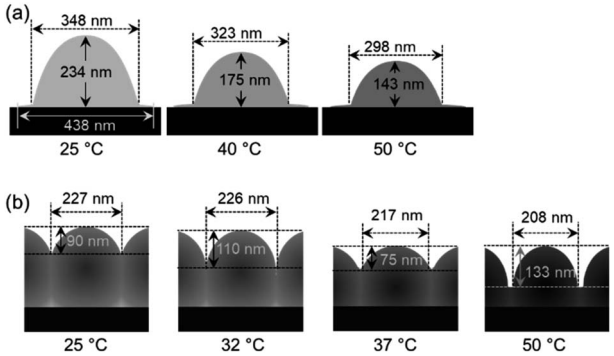

Scheme 1 Schematic illustration of the thermoresponsive behavior of the microgels on the substrate in (a) the isolated state and (b) the densely packed state.

Conclusions

In this study, the nanostructure and thermoresponsiveness of poly(NIPMAm-*co*-BIS) microgels, synthesized by precipitation polymerization, were evaluated using light scattering techniques and temperature-controllable high-speed atomic force microscopy (TC-HS-AFM) observations. These evaluations demonstrated that such pNIPMAm microgels have heterogeneous core–shell and non-thermoresponsive nanostructures in the core region, which is due to the mechanism of the precipitation polymerization. Static light scattering (SLS) and TC-HS-AFM measurements revealed a homogeneous cross-linking structure for the pNIPMAm microgels compared the pNIPAm microgels, and demonstrated that the structure of the microgels is affected by the monomer reactivity ratios. Furthermore, the thermoresponsiveness of microgels with different adsorption concentrations was investigated and the results showed that the thermoresponsiveness of densely packed microgels is suppressed by the compression and interpenetration of neighboring microgels. These findings can be expected to be useful in the design of stimuli-responsive coatings, such as those used as cell scaffolds.

Experimental

Materials

N-Isopropyl methacrylamide (NIPMAm, purity 97%) was purchased from Sigma-Aldrich and used as received. *N*,*N*′-Methylenebis(acrylamide) (BIS, 97%), sodium dodecyl sulfate (SDS, 95%), and potassium peroxodisulfate (KPS, 95%) were purchased from FUJIFILM Wako Pure Chemical Corporation (Japan) and used as received. Fluorosurf® was purchased from Fluoro Technology (Japan). Distilled ion-exchanged water used in the preparation of the microgels was obtained from EYELA, SA-2100E1.

Preparation of microgels by precipitation polymerization

Poly(NIPMAm-*co*-BIS) microgels were synthesized by aqueous free radical precipitation polymerizations, which were conducted in three-necked round bottom flasks (300 mL). The flasks were charged with NIPMAm (1.72 g), BIS (0.232 g), and water (90 mL), before a mechanical stirrer and condenser were installed. Then, the monomer solution was heated to 70 °C and sparged with nitrogen (30 min). Subsequently, an aqueous solution (5 mL) of SDS (0.0578 g) and an initiator solution (5 mL water and 0.0543 g KPS) were added in this order. After 4 h, the thus obtained microgel dispersions were cooled to room temperature to terminate the polymerization. Microgels were purified by two cycles of

centrifugation (415 000 × *g*)/redispersion in pure water and dialysis for a week (daily water changes).

Field emission scanning electron microscopy

The size uniformity of the microgels was evaluated by field emission scanning electron microscopy (FE-SEM, Hitachi Ltd., S-5000). For that purpose, microgel dispersions (2 μL; 0.002 wt%) were dried on a polystyrene substrate at room temperature. Prior to the measurements, Pt/Pd was sputtered onto the sample substrates (15 mA, 6 Pa, 80 s).

Light-scattering measurements

To evaluate the thermoresponsiveness of the hydrodynamic diameter (D_h) of the pNIPMAm microgels, dynamic light scattering (DLS) measurements were conducted (Malvern Instruments Ltd.; Zetasizer Nano S). The concentration of the microgel dispersions was approximately 0.002 wt%, and three individual measurements of 15 consecutive runs with 30 s of acquisition time were averaged. Prior to the measurements at each temperature, the samples were allowed to thermally equilibrate (10 min). The D_h of the microgels was derived from the obtained diffusion coefficients using the Stokes–Einstein equation (Zetasizer software v6.12).

The internal structure of the microgels in the dispersed state was evaluated by static light scattering (SLS) measurements using a DLS/SLS-5000 (ALV, Langen) and a He–Ne laser (632.8 nm, 22 mW). The scattering angle was changed from 30° to 90° and 15 individual measurements with 30 s of acquisition time were averaged. The concentration of the microgel dispersions was approximately 0.002 wt% and the samples were allowed to thermally equilibrate (10 min) prior to each measurement (25 °C and 50 °C). The scattering curves obtained from the SLS measurements were fitted by a fuzzy sphere form factor, $P(q)_{fuzzy}$:

$$P(q)_{\text{fuzzy}} = A\left[\frac{3[\sin(qR) - qR\cos(qR)]}{(qR)^3}\exp\left(-\frac{(\sigma_{\text{surf}}q)^2}{2}\right)\right]^2 \quad (1)$$

where, A, q, R, and σ_{surf} denote the scale values used to normalize the total scattering volume, the scattering vector, the radius of the particle where the scattering-length-density profile decreases to half the core density, and the width of the smeared particle surface (fuzzy layer), respectively.[45]

Electrophoresis analysis

The electrophoretic mobility (EPM) of the pNIPMAm microgels in the swollen and deswollen state dispersed in an aqueous NaCl solution (1 mM) was evaluated using a Zetasizer Nano ZS system (Malvern, Zetasizer software Ver. 7.12). Three individual measurements of 20 consecutive runs with 120 mV were averaged. The concentration of the microgel dispersions was approximately 0.01 wt% and the samples were allowed to thermally equilibrate (10 min) prior to the measurements at 25 °C and 50 °C.

TC-HS-AFM observations

A laboratory-built HS-AFM operated in tapping mode was used in this study.[44] As a AFM cantilever, a miniaturized cantilever (BL-AC10-DS, Olympus, Japan) was used (spring constant: ~0.1 N m^{-1}, quality factor: ~2, resonant frequency: ~600 kHz in water). The cantilever was vibrated at near the resonance frequency and its oscillation amplitude was detected by a fast amplitude detector through an optical-beam-deflection detector with a red laser (680 nm). To gain a sharp AFM probe, a carbon pillar was deposited by electron-beam deposition and that was subsequently sharpened by plasma etching under argon environment, resulting in an end radius of ~4 nm. For the HS-AFM observation of the microgels and microgel sheets, the free-oscillation amplitude of the cantilever far from the sample surface was set to 5–30 nm, and the set-point amplitude was set to 70–90% of the free-oscillation amplitude, depending on the size and concentration of the microgels.

In addition to the topographic imaging, phase shifts of the cantilever oscillation detected by a lock-in amplifier (HF2LI, Zurich Instruments AG, Switzerland) were imaged simultaneously. The excitation signal was used as the reference of the lock-in detection and the time constant was 20 μs.

In order to adsorb the pNIPMAm microgels on the substrates, a hydrophobized mica substrate was used. For that purpose, Fluorosurf® (0.5 μL) was dropped on freshly cleaved mica and dried at room temperature to produce a hydrophobic fluororesin thin film. Subsequently, pNIPMAm microgel dispersions or pastes of different concentrations were dropped on the hydrophobized mica substrates. After 5 min, excess microgels were thoroughly removed by washing with pure water.

The thermoresponsiveness of the microgels with different adsorption concentrations was visualized using TC-HS-AFM.[48]

The solution temperature was increased by passing a DC current through the conductive indium tin oxide (ITO) glass at the bottom of the solution pool of the cantilever holder. The solution temperature, measured using thermocouples installed near the cantilever, can be increased by 2.0 °C min^{-1} *via* software feedback control.

Author contributions

Y. N. and D. S. wrote the draft manuscript. Y. N. evaluated the microgels using TC-HS-AFM; the obtained data were analyzed by Y. N., T. I., and H. M. T. I. contributed to the preparation and characterization of the microgels. I. S., T. K., and M. S. contributed to the SLS measurements. T. U. contributed to the development/tuning of the TC-HS-AFM. D. S. designed and supervised the study.

Conflicts of interest

The authors declare the absence of any potential conflicts of interest.

Acknowledgements

D. S. acknowledges a Grant-in-Aid for Young Scientists (A) (JSPS; 17H04892) and a Grant-in-Aid for Scientific Research on Innovative Areas (19H05388) from the Japanese Ministry of Education, Culture, Sports, Science, and Technology (MEXT). T. U. acknowledges Grants-in-Aid for Scientific Research on Innovative Areas (19H05389, 20H04669) from MEXT. Y. N. acknowledges a fellowship from the Japan Society for the Promotion of Science (JSPS; 20J1272700).

References

1 R. Pelton, *Adv. Colloid Interface Sci.*, 2000, **85**, 1.
2 F. A. Plamper and W. Richtering, *Acc. Chem. Res.*, 2017, **50**, 131.
3 D. Suzuki, K. Horigome, T. Kureha, S. Matsui and T. Watanabe, *Polym. J.*, 2017, **49**, 695.
4 M. Karg, A. Pich, T. Hellweg, T. Hoare, L. A. Lyon, J. J. Crassous, D. Suzuki, R. A. Gumerov, S. Schneider, I. I. Potemkin and W. Richtering, *Langmuir*, 2019, **35**, 6231.
5 N. M. B. Smeets and T. Hoare, *J. Polym. Sci., Part A: Polym. Chem.*, 2013, **51**, 3027.
6 W. Richtering, I. I. Potemkin, A. A. Rudov, G. Sellge and C. Trautwein, *Nanomedicine*, 2016, **11**, 2879.
7 J. C. Cuggino, E. R. Osorio Blanco, L. M. Gugliotta, C. I. Alvarez Igarzabal and M. J. Calderón, *J. Controlled Release*, 2019, **307**, 221.
8 Y. Hoshino, K. Imamura, M. Yue, G. Inoue and Y. Miura, *J. Am. Chem. Soc.*, 2012, **134**, 18177.
9 T. Kureha, Y. Nishizawa and D. Suzuki, *ACS Omega*, 2017, **2**, 7686.
10 T. Kureha and D. Suzuki, *Langmuir*, 2018, **34**, 837.
11 S. Matsui, K. Hosho, H. Minato, T. Uchihashi and D. Suzuki, *Chem. Commun.*, 2019, **55**, 10064.
12 Y. Lu and M. Ballauff, *Prog. Polym. Sci.*, 2011, **36**, 767.
13 S. Wu, J. Dzubiella, J. Kaiser, M. Drechsler, X. Guo, M. Ballauff and Y. Lu, *Angew. Chem., Int. Ed.*, 2012, **51**, 2229.
14 T. Kureha, Y. Nagase and D. Suzuki, *ACS Omega*, 2018, **3**, 6158.
15 Y. Xia, X. He, M. Cao, C. Chen, H. Xu, F. Pan and J. R. Lu, *Biomacromolecules*, 2013, **14**, 3615.
16 S. Saxena, C. E. Hansen and L. A. Lyon, *Acc. Chem. Res.*, 2014, **47**, 2426.
17 J. Kim, S. Nayak and L. A. Lyon, *J. Am. Chem. Soc.*, 2005, **127**, 9588.
18 M. Wei, Y. Gao, X. Li and M. J. Serpe, *Polym. Chem.*, 2017, **8**, 127.
19 T. Ngai, S. H. Behrens and H. Auweter, *Chem. Commun.*, 2005, 331.
20 T. Watanabe, M. Takizawa, H. Jiang, T. Ngai and D. Suzuki, *Chem. Commun.*, 2019, **55**, 5990.
21 D. Suzuki, T. Kobayashi, R. Yoshida and T. Hirai, *Soft Matter*, 2012, **8**, 11447.
22 S. Matsui, K. Inui, Y. Kumai, R. Yoshida and D. Suzuki, *ACS Biomater. Sci. Eng.*, 2019, **5**, 5615.
23 K. Inui, T. Watanabe, H. Minato, S. Matsui, K. Ishikawa, R. Yoshida and D. Suzuki, *J. Phys. Chem. B*, 2020, **124**, 3828.
24 R. H. Pelton and P. Chibante, *Colloids Surf.*, 1986, **20**, 247.
25 B. Wedel, Y. Hertle, O. Wrede, J. Bookhold and T. Hellweg, *Polymers*, 2016, **8**, 162.
26 O. Wrede, S. Bergmann, Y. Hannappel, T. Hellweg and T. Huser, *Soft Matter*, 2020, **16**, 8078.
27 J. Maldonado-Valderrama, T. del Castillo-Santaella, I. Adroher-Benítez, A. Moncho-Jordá and A. Martín-Molina, *Soft Matter*, 2017, **13**, 230.
28 F. A. L. Janssen, M. Kather, A. Ksiazkiewicz, A. Pich and A. Mitsos, *ACS Omega*, 2019, **4**, 13795.
29 T. Cai, M. Marquez and Z. Hu, *Langmuir*, 2007, **23**, 8663.
30 D. Duracher, A. ElaÏssari and C. Pichot, *Colloid Polym. Sci.*, 1999, **277**, 905.
31 I. Berndt, J. S. Pedersen, P. Lindner and W. Richtering, *Langmuir*, 2006, **22**, 459.
32 D. Suzuki and R. Yoshida, *Polym. J.*, 2010, **42**, 501.
33 M. H. Smith, E. S. Herman and L. A. Lyon, *J. Phys. Chem. B*, 2011, **115**, 3761.
34 K. von Nessen, M. Karg and T. Hellweg, *Polymer*, 2013, **54**, 5499.
35 D. Suzuki and K. Horigome, *J. Phys. Chem. B*, 2013, **117**, 9073.
36 K. Urayama, T. Saeki, S. Cong, S. Uratani, T. Takigawa, M. Murai and D. Suzuki, *Soft Matter*, 2014, **10**, 9486.
37 T. Kureha, D. Aoki, S. Hiroshige, K. Iijima, D. Aoki, T. Takata and D. Suzuki, *Angew. Chem., Int. Ed.*, 2017, **56**, 15393.
38 M. Takizawa, Y. Sazuka, K. Horigome, Y. Sakurai, S. Matsui, H. Minato, T. Kureha and D. Suzuki, *Langmuir*, 2018, **34**, 4515.
39 M. Keerl, J. S. Pedersen and W. Richtering, *J. Am. Chem. Soc.*, 2009, **131**, 3093.
40 A. Balaceanu, V. Mayorga, W. Lin, M.-P. Schürings, D. E. Demco, A. Böker, M. A. Winnik and A. Pich, *Colloid Polym. Sci.*, 2013, **291**, 21.
41 K. C. Clarke and L. A. Lyon, *Langmuir*, 2013, **29**, 12852.
42 Y. Wu, S. Wiese, A. Balaceanu, W. Richtering and A. Pich, *Langmuir*, 2014, **30**, 7660.
43 S. Nayak and L. A. Lyon, *Angew. Chem., Int. Ed.*, 2005, **44**, 7686.
44 Y. Nishizawa, H. Minato, T. Inui, T. Uchihashi and D. Suzuki, *Langmuir*, 2021, **37**, 151.
45 M. Stieger, W. Richtering, J. S. Pedersen and P. Lindner, *J. Chem. Phys.*, 2004, **120**, 6197.
46 B. R. Saunders, *Langmuir*, 2004, **20**, 3925.
47 R. Keidel, A. Ghavami, D. M. Lugo, G. Lotze, O. Virtanen, P. Beumers, J. S. Pedersen, A. Bardow, R. G. Winkler and W. Richtering, *Sci. Adv.*, 2018, **4**, eaao7086.
48 A. Mourran, Y. Wu, R. A. Gumerov, A. A. Rudov, I. I. Potemkin, A. Pich and M. Möller, *Langmuir*, 2016, **32**, 723.
49 G. M. Conley, S. Nöjd, M. Braibanti, P. Schurtenberger and F. Scheffold, *Colloids Surf., A*, 2016, **499**, 18.
50 X. Wu, R. H. Pelton, A. E. Hamielec, D. R. Woods and W. McPhee, *Colloid Polym. Sci.*, 1994, **272**, 467.
51 S. Matsui, Y. Nishizawa, T. Uchihashi and D. Suzuki, *ACS Omega*, 2018, **3**, 10836.

52 K. Honda, Y. Sazuka, K. Iizuka, S. Matsui, T. Uchihashi, T. Kureha, M. Shibayama, T. Watanabe and D. Suzuki, *Angew. Chem., Int. Ed.*, 2019, **58**, 7294.
53 Y. Nishizawa, S. Matsui, K. Urayama, T. Kureha, M. Shibayama, T. Uchihashi and D. Suzuki, *Angew. Chem., Int. Ed.*, 2019, **58**, 8809.
54 H. Minato, Y. Nishizawa, T. Uchihashi and D. Suzuki, *Polym. J.*, 2020, **52**, 1137.
55 Y. Nishizawa, K. Honda and D. Suzuki, *Chem. Lett.*, DOI: 10.1246/cl.210028.
56 J. Brandup, E. H. Immergut, E. A. Grulke, A. Abe and D. R. Bloch, *Polymer Handbook*, Wiley, New York, 4th edn, 1999.
57 J. Baselga, M. A. Llorente, J. L. Nieto, I. Hernánndez-Fuentes and I. F. Piérola, *Eur. Polym. J.*, 1988, **24**, 161.
58 M. Cors, L. Wiehemeier, Y. Hertle, A. Feoktystov, F. Cousin, T. Hellweg and J. Oberdisse, *Langmuir*, 2018, **34**, 15403.
59 T. Ando, T. Uchihashi and S. Scheuring, *Chem. Rev.*, 2014, **114**, 3120.
60 L. H. Alvarez, S. Eisold, R. A. Gumerov, M. Strauch, A. A. Rudov, P. Lenssen, D. Merhof, I. I. Potemkin, U. Simon and D. Wöll, *Nano Lett.*, 2019, **19**, 8862.
61 G. M. Conley, P. Aebischer, S. Nöjd, P. Schurtenberger and F. Scheffold, *Sci. Adv.*, 2017, **3**, e1700969.
62 G. M. Conley, C. Zhang, P. Aebischer, J. L. Harden and F. Scheffold, *Nat. Commun.*, 2019, **10**, 2436.